

Multi-strange baryon production in p-Pb collisions at $\sqrt{s_{NN}}=5.02$

(ALICE Collaboration) Adam, J.; ...; Antičić, Tome; ...; Erhardt, Filip; ...; Gotovac, Sven; ...; Mudnić, Eugen; ...; ...

Source / Izvornik: **Physics Letters B**, 2016, 758, 389 - 401

Journal article, Published version

Rad u časopisu, Objavljena verzija rada (izdavačev PDF)

<https://doi.org/10.1016/j.physletb.2016.05.027>

Permanent link / Trajna poveznica: <https://urn.nsk.hr/urn:nbn:hr:217:041120>

Rights / Prava: [Attribution 4.0 International](#)/[Imenovanje 4.0 međunarodna](#)

Download date / Datum preuzimanja: **2024-11-14**



Repository / Repozitorij:

[Repository of the Faculty of Science - University of Zagreb](#)



Multi-strange baryon production in p–Pb collisions at $\sqrt{s_{NN}} = 5.02$ TeV

ALICE Collaboration*

ARTICLE INFO

Article history:

Received 16 January 2016
 Received in revised form 10 May 2016
 Accepted 10 May 2016
 Available online 12 May 2016
 Editor: L. Rolandi

ABSTRACT

The multi-strange baryon yields in Pb–Pb collisions have been shown to exhibit an enhancement relative to pp reactions. In this work, Ξ and Ω production rates have been measured with the ALICE experiment as a function of transverse momentum, p_T , in p–Pb collisions at a centre-of-mass energy of $\sqrt{s_{NN}} = 5.02$ TeV. The results cover the kinematic ranges $0.6 \text{ GeV}/c < p_T < 7.2 \text{ GeV}/c$ and $0.8 \text{ GeV}/c < p_T < 5 \text{ GeV}/c$, for Ξ and Ω respectively, in the common rapidity interval $-0.5 < y_{CMS} < 0$. Multi-strange baryons have been identified by reconstructing their weak decays into charged particles. The p_T spectra are analysed as a function of event charged-particle multiplicity, which in p–Pb collisions ranges over one order of magnitude and lies between those observed in pp and Pb–Pb collisions. The measured p_T distributions are compared to the expectations from a Blast-Wave model. The parameters which describe the production of lighter hadron species also describe the hyperon spectra in high multiplicity p–Pb collisions. The yield of hyperons relative to charged pions is studied and compared with results from pp and Pb–Pb collisions. A continuous increase in the yield ratios as a function of multiplicity is observed in p–Pb data, the values of which range from those measured in minimum bias pp to the ones in Pb–Pb collisions. A statistical model qualitatively describes this multiplicity dependence using a canonical suppression mechanism, in which the small volume causes a relative reduction of hadron production dependent on the strangeness content of the hyperon.

© 2016 The Author(s). Published by Elsevier B.V. This is an open access article under the CC BY license (<http://creativecommons.org/licenses/by/4.0/>). Funded by SCOAP³.

1. Introduction

Collisions of heavy nuclei at ultra-relativistic energies allow the study of a deconfined state of matter, the Quark–Gluon Plasma, in which the degrees of freedom are partonic, rather than hadronic. The role of strange hadron yields in searching for this state was pointed out at an early stage [1]. It was subsequently found that in high energy nucleus–nucleus (A–A) collisions at the Super Proton Synchrotron (SPS), the Relativistic Heavy Ion Collider (RHIC) and the Large Hadron Collider (LHC) the abundances of strange and multi-strange baryons are compatible with those from thermal statistical model calculations [2–10].

In smaller collision systems at the same centre-of-mass energies, in particular proton–proton (pp) collisions, the relative abundance of multi-strange baryons is lower with respect to A–A collisions, whether normalised to participant nucleons or produced particles (pions or charged hadrons). This led to the interpretation that strangeness enhancement is observed in A–A collisions. Attempts to explain this phenomenon include the application of a canonical formalism in the statistical model, replacing the grand canonical approach, in which the requirement to conserve

the strangeness quantum number when producing (multi-)strange baryons in small systems is imposed [11]. This means that strange hadrons are produced with a lower relative abundance in small systems, an effect known as canonical suppression. Such a theoretical framework has been used to make predictions for LHC energies [12]. Further complications in the interpretation arise when the produced system, although small, is formed in peripheral A–A collisions where the particle production may not be from a contiguous volume due to core–corona effects [13,14]. Evidence for this effect was seen at RHIC where a canonical suppression calculation based on the estimated number of participant nucleons could not successfully reproduce the data [15]. A cleaner way to investigate canonical suppression effects is provided by proton–nucleus (p–A) collisions.

Proton–nucleus collisions provide an opportunity to study the p_T -dependence of the particle spectra created in a system with a different, more compact, initial geometry than A–A collisions where a similar number of charged particles are produced. Studying this dependence is important in determining the applicability of hydrodynamics [16] which has been successful in describing the particle spectra in A–A collisions [17–19].

At the LHC the combination of the rise in particle production per nucleon–nucleon collision with increasing \sqrt{s} and a dedicated p–Pb data-taking period have enabled the ALICE experiment to

* E-mail address: alice-publications@cern.ch.

collect a large sample of Ξ^\pm and Ω^\pm . In this Letter, we set out the methods for these studies, present the results obtained and discuss how they fit into a theoretical picture.

2. Sample and data analysis

The results presented in this Letter were obtained from a sample of the data collected with the ALICE detector [20] during the LHC p–Pb run at $\sqrt{s_{NN}} = 5.02$ TeV in the beginning of 2013. The two scintillator arrays VOA (direction of Pb beam), and V0C (direction of p beam), covering pseudo-rapidity ranges of $2.8 < \eta < 5.1$ and $-3.7 < \eta < -1.7$, respectively, served both as triggering detectors and for determining the event multiplicity class [21]. The tracking of particles in the central barrel, covering $|\eta| < 0.9$, takes place in the Inner Tracking System (ITS), which consists of the two innermost silicon pixel layers, surrounded by two silicon drift and two silicon strip layers, all placed within a radius of 43 cm, and the Time Projection Chamber (TPC), a large cylindrical drift chamber filled with a Ne–CO₂ gas mixture [20]. Measurements of the energy loss by charged particles in the gas allow particles to be identified with this detector.

A trigger requiring a coincidence within less than 1 ns in the V0 detectors selected around 100 million events, which are mainly non-single diffractive (NSD) events and contain a negligible contribution from single diffractive (SD) and electromagnetic (EM) processes [22]. A dedicated radiator-quartz detector (T0) provided a measurement of the event time of the collisions. The V0 and T0 time resolutions allowed discrimination of beam–beam interactions from background events in the interaction region. Further background suppression was applied in the offline analysis using time information from the neutron Zero Degree Calorimeter on the Pb-going side. Primary vertices (PVs) were selected if their position along the beam axis was reconstructed within 10 cm of the geometrical centre of the detector. In Monte Carlo (MC) studies an efficiency of 99.2% for this trigger was obtained, while the joint trigger and primary vertex reconstruction efficiency lies at 97.8% [22]. The estimated mean number of interactions per bunch crossing was below 1% in the sample chosen for this analysis.

The analysed events were divided into seven multiplicity percentile classes according to the total number of particles measured in the forward VOA detector. The efficiency-corrected mean number of charged primary particles per unit rapidity ($\langle dN_{ch}/d\eta \rangle$) within $-0.5 < \eta < 0.5$ in the laboratory reference frame for each of these multiplicity bins were published in [23].

Due to the asymmetric energies of the proton and lead ion beams, a consequence of the 2-in-1 magnet design of the LHC, the nucleon–nucleon centre-of-mass system is shifted by 0.465 units of rapidity in the direction of the proton beam with respect to the laboratory frame. The measurements reported in this Letter were performed in the central rapidity window defined in the centre-of-mass frame within $-0.5 < y < 0$, where negative rapidity corresponds to the side of the detector into which the Pb beam travels.

The identification of multi-strange baryons was based on the topology of their weak decays through the reconstruction of the tracks left behind by the decay products, referred to as the daughter particles. The daughters of the $\Xi^- \rightarrow \Lambda \pi^-$ (BR: 99.9%), $\Omega^- \rightarrow \Lambda K^-$ (BR: 67.8%) and the subsequent $\Lambda \rightarrow p \pi^-$ (BR: 63.9%) weak decays [24], as well as the corresponding decays of the Ξ^+ and Ω^+ , were reconstructed by combining track information from the TPC and the ITS [25]. Proton, anti-proton and charged π and K tracks were identified in the TPC via their measured energy deposition, which was compared with a mass-dependent parameterisation of ionisation loss in the TPC gas as a function of momentum [26]. All daughter candidates were required to lie within 4σ of

Table 1

The parameters for V^0 (Λ and $\bar{\Lambda}$) and cascades (Ξ^\pm and Ω^\pm) selection criteria. Where a criterion for Ξ^\pm and Ω^\pm finding differs, the value for the Ω^\pm case is in parentheses. DCA represents “distance of closest approach,” PV the primary vertex, θ is the angle between the momentum vector of the reconstructed V^0 or cascade, and the displacement vector between the decay and primary vertices. The curvature of the cascade particle’s trajectory is neglected.

V ⁰ finding criteria	
DCA: h^\pm to PV	> 0.04 (0.03) cm
DCA: h^- to h^+	< 1.5 standard deviations
Λ mass (m_{V0})	$1.108 < m_{V0} < 1.124$ GeV/ c^2
Fiducial volume (R_{2D})	$R_{2D} > 1.1$ (1.2) cm
V ⁰ pointing angle	$\cos\theta_{V0} > 0.97$
Cascade finding criteria	
Proper decay length	< 3 × mean decay length
DCA: π^\pm (K^\pm) to PV	> 0.04 cm
DCA: V ⁰ to PV	> 0.06 cm
DCA: π^\pm (K^\pm) to V ⁰	< 1.3 cm
Fiducial volume (R_{2D})	$R_{2D} > 0.5(0.6)$ cm
Cascade pointing angle	$\cos\theta_{casc} > 0.97$

their characteristic Bethe–Bloch energy loss curve. Multi-strange candidates were selected through the geometrical association of the V^0 component (Λ or $\bar{\Lambda}$ decay) to a further secondary, ‘bachelor’ track (identified as π^\pm or K^\pm). In this process, several geometrical variables were measured for each candidate, and criteria were set on them in order to purify the selected sample: numerical values for the selection cuts applied are reported in Table 1. These selections are similar to those in the pp measurements [25], a consequence of the low multiplicities present in the detector in the p–Pb collisions. As a result the correction factors for the efficiency are also similar. In addition to the settings on topological variables, a cut has been applied on the V^0 invariant mass window of ± 8 MeV/ c^2 from the nominal Λ mass [24]. Further restrictions were set on the proper lifetime of the Ξ^\pm and Ω^\pm . By requiring this variable to be less than 3 times the mean decay length (4.91 cm and 2.46 cm, respectively), we discarded low-momentum secondary particles and false multi-strange candidates, the daughter tracks of which originated from interactions with detector material.

The invariant mass of the Ξ and Ω hyperons was calculated by assuming the known masses [24] of the Λ and of the bachelor track. The mass was reconstructed twice for each cascade candidate, once assuming the bachelor to be a π and once a K. This allowed the removal of an important fraction of the Ω background, which contained a large contribution from the Ξ candidates that pass the Ω selection criteria. Most of these false Ω were removed discarding all candidates that could be reconstructed as Ξ with a mass within 10 MeV/ c^2 of the known mass [24] of the Ξ baryon. Fig. 1 shows the invariant mass distributions for the Ξ^- and Ω^- hadrons in well populated p_T bins for the lowest and highest multiplicity classes.

For the signal extraction, a peak region was defined within 4σ of the mean of a Gaussian invariant mass peak for every measured p_T interval. Adjacent background bands, covering an equal combined mass interval as the peak region, were defined on both sides of that central region. This is illustrated in Fig. 1 with the shaded bands on either side of the peak. The number of bin entries inside the side-bands was subtracted from the number of candidates within the peak region, assuming the background to be linear across the mass range considered.

The p_T distributions were corrected for detector acceptance and reconstruction efficiencies. These were estimated with the use of DPMJet [27] simulated Monte Carlo (MC) events, which were propagated through the detector with GEANT3 [28].

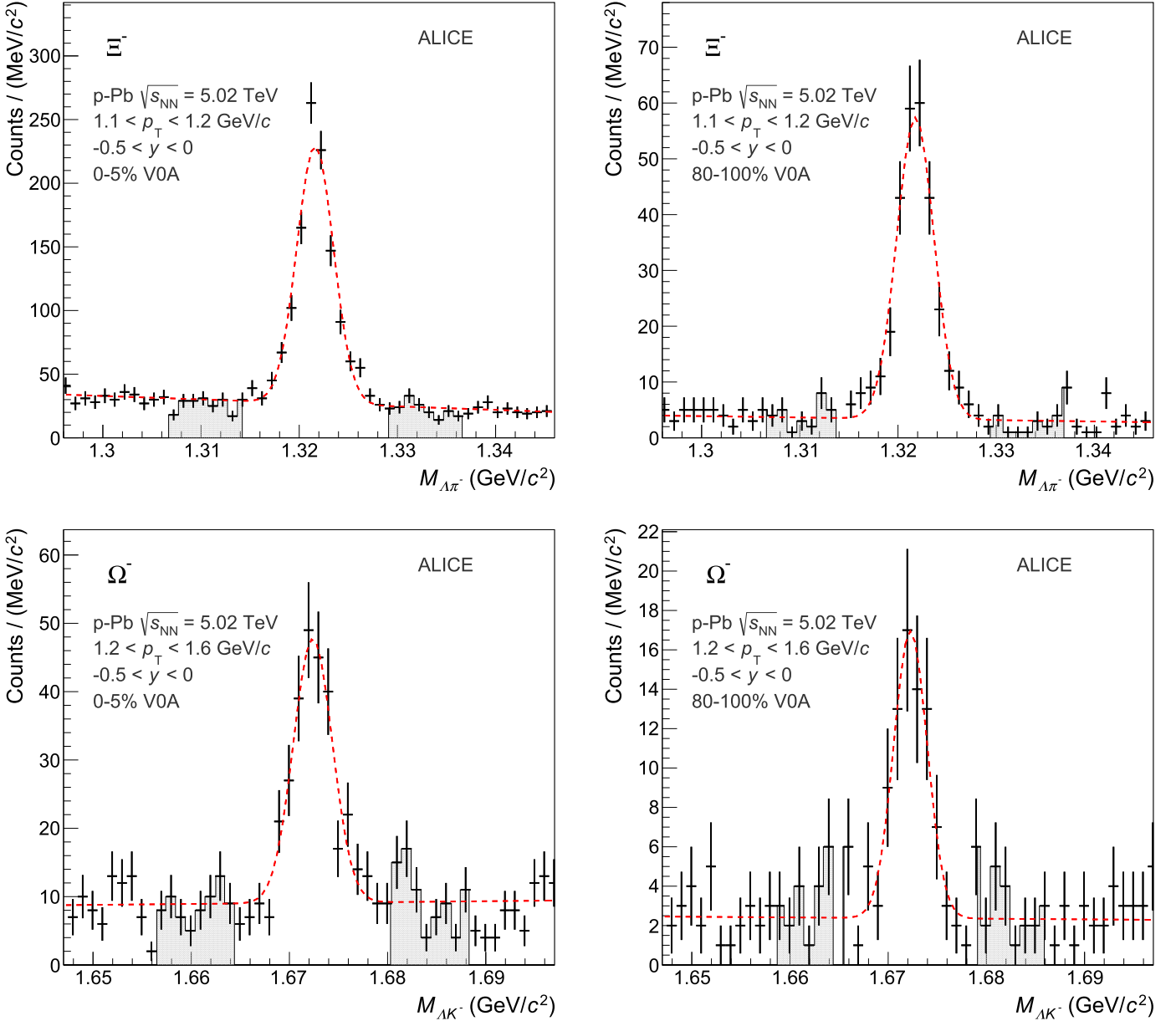


Fig. 1. Invariant mass distributions of the Ξ^- and Ω^- in the 1.1–1.2 GeV/c and 1.2–1.6 GeV/c p_T bins respectively, fitted with a Gaussian peak and linear background (dashed red curves). The distributions for highest (left) and lowest (right) multiplicity classes are shown. The fits only serve to illustrate the peak position with respect to which the bands were defined and the linear background assumption for the applied signal extraction method.

2.1. Systematic uncertainties

Systematic uncertainties due to the choice of selection criteria were examined separately in each p_T interval of the measured spectra. Individual settings were loosened and tightened, in order to measure changes in the signal loss correction. For the Ξ hyperons, the signal extraction accounts for an uncertainty of around 2% but reaches 5% at low- p_T and in high multiplicity events, while for the Ω , uncertainties of 3–5% were measured. The uncertainty due to the topological selections is around 2(3)% for the main p_T region, and up to 3(5)% at low momentum for $\Xi(\Omega)$. The constraint on the V^0 mass window contributes to the total uncertainty with around 0.5(1)% and both the TPC tracking and identification cuts with 2(3)%. The proper decay length cut gives another 3(5)% uncertainty at low p_T . A 4% error was added due to the material budget, and for the Ω^\pm only, an additional 3% due to the mass hypothese-

sis cut. All these individual error contributions, which are listed in Table 2, are added in quadrature. Apart from the low momentum region, no p_T dependence is observed in the total uncertainty. The total systematic error lies between 5–6(8)% across the whole spectrum, reaching up to 8(14)% in the lowest p_T bins for the $\Xi(\Omega)$ baryons.

The fraction of the systematic error that is uncorrelated across multiplicity was calculated by using the same method applied in [23], in which spectra deviations in specific multiplicity classes were compared to those observed in the integrated data sample. The choice of the topological parameter values and the applied signal extraction method generates the dominant contribution to the uncorrelated uncertainties across multiplicity. These uncertainties were measured to be within 2% in the case of the Ξ and 3% in the case of the Ω , which constitutes a fraction that lies between 20 and 40% of the total systematic uncertainties.

Table 2

Contributions to the total systematic uncertainties for the Ξ^\pm and Ω^\pm spectra measurements. The values in brackets indicate the maximum uncertainties measured for low- p_T cascades (see text).

Source	Ξ^\pm	Ω^\pm
Material budget	4%	4%
Competing mass hypothesis	–	3%
Topological variables	2–3(5)%	3–5%
Signal extraction	2(5)%	3(5)%
Particle identification	2%	3%
Track selection	2%	3%
Proper decay length	1(3)%	2(5)%
V^0 mass window	0.5%	1%

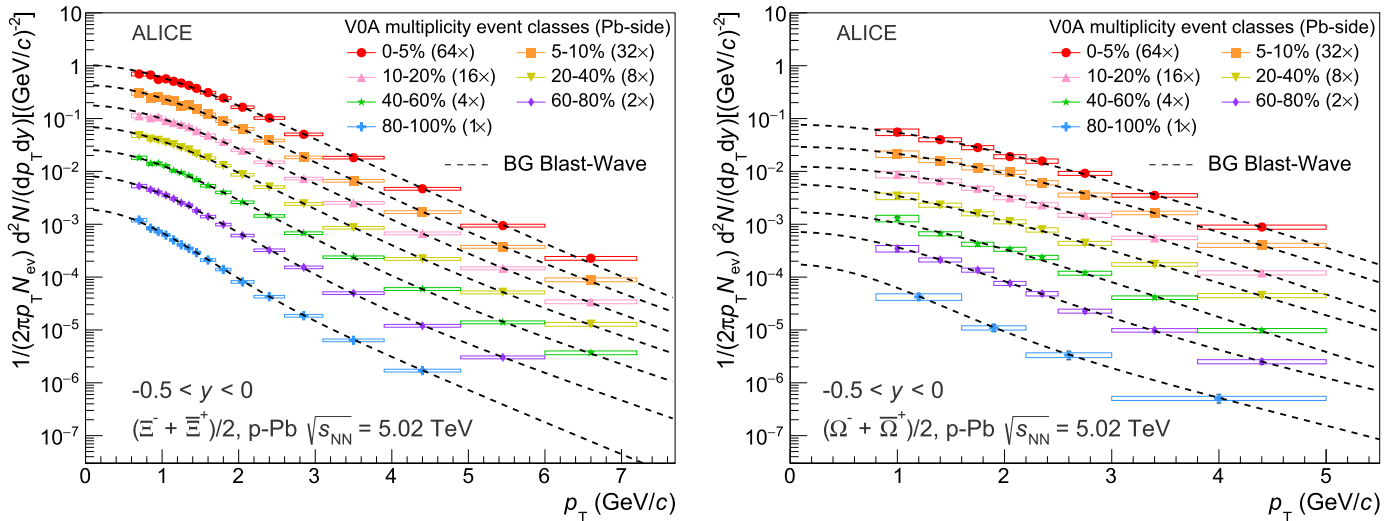


Fig. 2. (Colour online.) Invariant p_T -differential yields of $(\Xi^- + \Xi^+)/2$ and $(\Omega^- + \Omega^+)/2$ in different multiplicity classes. Data have been scaled by successive factors of 2 for better visibility. Statistical (bars), full systematic (boxes) and uncorrelated across multiplicity (transparent boxes) uncertainties are plotted. The dashed curves represent Blast-Wave fits to each individual distribution.

3. Results

3.1. Transverse momentum spectra

The p_T distributions of Ξ^- , Ξ^+ , Ω^- and Ω^+ in $-0.5 < y < 0$ are shown in Fig. 2 for different multiplicity intervals, as defined in [23]. Since antiparticle and particle spectra are identical within uncertainties, the average of the two is shown. The spectra exhibit a progressive flattening with increasing multiplicity, which is qualitatively reminiscent of what is observed in Pb–Pb collisions [10].

The calculation of p_T -integrated yields can be performed by using data in the measured region and a parametrisation-based extrapolation elsewhere. The Boltzmann–Gibbs Blast-Wave (BG–BW) model [16] gives a good description of each p_T spectrum and has been used as a tool for this extrapolation. Other alternatives, such as the Levy–Tsallis [29] and Boltzmann distributions, were used for estimating the systematic uncertainty due to the extrapolation.

The extrapolation in the unmeasured Ξ^\pm (Ω^\pm) low- p_T region grows progressively with decreasing multiplicity, from around 16%(19%) of the total yield in the 0–5% multiplicity class to around 27%(40%) in the 80–100% class. The systematic uncertainty assigned to the yield due to the extrapolation technique is 2.8%(7.8%) for high multiplicities and rises to 5.2%(14.5%) in the case where the fraction of the extrapolated yield is highest.

3.2. Comparison to Blast-Wave model

In order to investigate whether the observed spectral shapes are consistent with a system that exhibits hydrodynamical radial

expansion, the measured distributions have been further studied in the context of the BG–BW model [16]. This model assumes a locally thermalised medium that expands collectively with a common velocity field and then undergoes an instantaneous freeze-out. In this framework, a simultaneous fit to identified particle spectra allows for the determination of common freeze-out parameters. These can be used to predict the p_T distribution for other particle species in a collective expansion picture. It should be noted that such a simultaneous fit differs from the individual fits mentioned in the previous section and used only for extrapolating the spectra.

The Ξ^- , Ξ^+ , Ω^- and Ω^+ p_T spectra in the 0–5% and 80–100% multiplicity classes are compared to predictions from the BG–BW model with parameters acquired from a simultaneous fit to π^\pm , K^\pm , $p(\bar{p})$ and $\Lambda(\bar{\Lambda})$ in Fig. 3 [23]. The model describes the measured shapes within uncertainties up to a p_T of approximately 4 GeV/c for Ξ and 5 GeV/c for Ω in the highest multiplicity class. This indicates that multi-strange hadrons also follow a common motion with the lighter hadrons and is suggestive of the presence of radial flow in p–Pb collisions. However, it is worth noting that some final state effects could also modify the spectra in a similar manner to radial flow. For example, PYTHIA [30] implements the colour reconnection mechanism, which fuses strings originating from independent parton interactions, leading to fewer but more energetic hadrons, which has been shown to mimic radial flow [31].

Applying the same technique to results from the lower multiplicity classes reveals that the agreement of the data with the

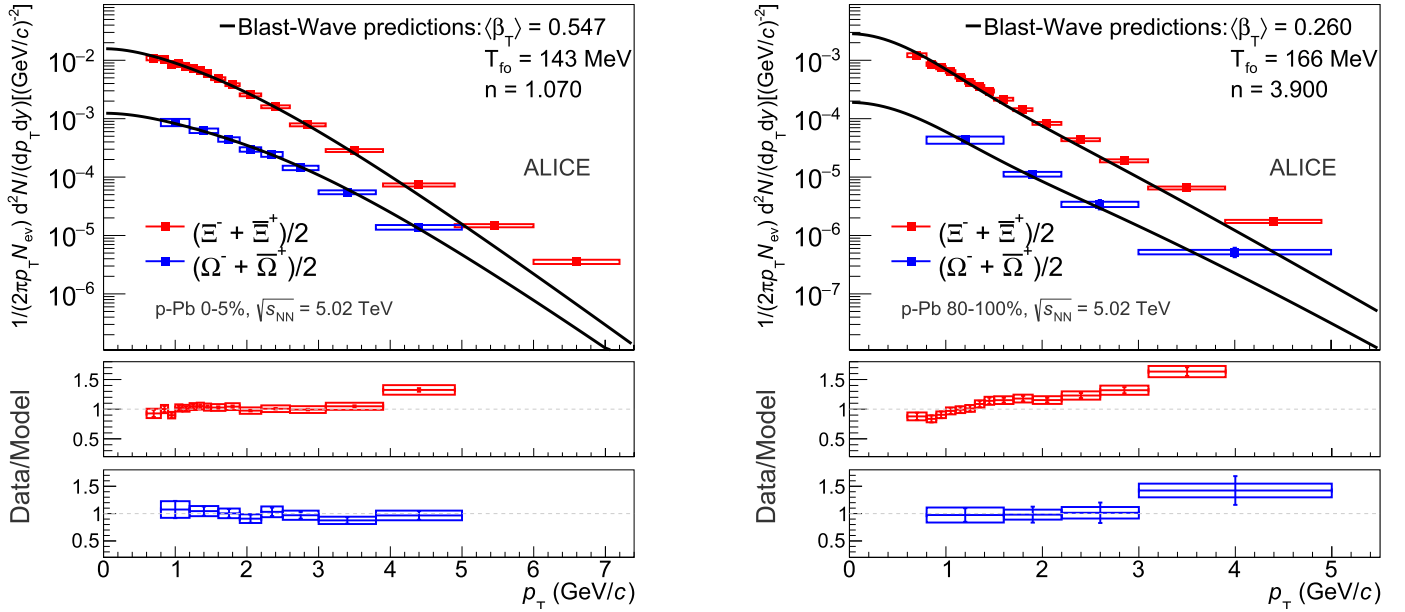


Fig. 3. (Colour online.) $(\Xi^- + \Xi^+)/2$ and $(\Omega^- + \Omega^+)/2$ p_T spectra in the 0–5% (left) and 80–100% (right) multiplicity classes compared to predictions from the BG–BW model (upper panels) with the ratios on a linear scale (lower panels). The parameters are based on simultaneous fits to lighter hadrons [23]. See text for details.

Table 3

The mid-rapidity $\langle dN_{ch}/d\eta \rangle$ values for each of the 7 multiplicity classes and the $\Xi^- + \Xi^+$ and $\Omega^- + \Omega^+$ integrated yields per unit rapidity normalised to the visible cross section. The statistical uncertainty on the yields is followed by the systematic uncertainty.

Event class	$\langle dN_{ch}/d\eta \rangle$ $ \eta_{lab} < 0.5$	$dN/dy(\Xi^- + \Xi^+)$	$dN/dy(\Omega^- + \Omega^+)$
0–5%	45 ± 1	$0.2354 \pm 0.0020 \pm 0.0161$	$0.0260 \pm 0.0011 \pm 0.0034$
5–10%	36.2 ± 0.8	$0.1861 \pm 0.0016 \pm 0.0138$	$0.0215 \pm 0.0008 \pm 0.0029$
10–20%	30.5 ± 0.7	$0.1500 \pm 0.0010 \pm 0.0112$	$0.0167 \pm 0.0006 \pm 0.0022$
20–40%	23.2 ± 0.5	$0.1100 \pm 0.0006 \pm 0.0085$	$0.0120 \pm 0.0005 \pm 0.0016$
40–60%	16.1 ± 0.4	$0.0726 \pm 0.0006 \pm 0.0065$	$0.0072 \pm 0.0003 \pm 0.0010$
60–80%	9.8 ± 0.24	$0.0398 \pm 0.0004 \pm 0.0031$	$0.0042 \pm 0.0002 \pm 0.0006$
80–100%	4.3 ± 0.1	$0.0143 \pm 0.0003 \pm 0.0015$	$0.0013 \pm 0.0003 \pm 0.0003$

Blast-Wave predictions become progressively worse. The comparison between lowest and highest multiplicity cases can be seen in Fig. 3, where their respective ratios to the model predictions are shown in the lower panels. These observations indicate that common kinetic freeze-out conditions are able to better describe the spectra in high multiplicity p–Pb collisions.

The multi-strange baryon spectra in central Pb–Pb collisions [10] have also been investigated in a common freeze-out scenario [17,18] and similar studies were performed for Au–Au collisions [19]. In contrast to high multiplicity p–Pb collisions, where all stable and long-lived hadron spectra are compatible with a single set of kinetic freeze-out conditions (the temperature T_{fo} and the mean transverse flow velocity $\langle\beta_T\rangle$), multi-strange particles in central heavy-ion collisions seem to experience less transverse flow and may freeze out earlier in the evolution of the system when compared to most of the other hadrons.

3.3. Hyperon to pion ratios

The measured integrated yields in the seven multiplicity classes are given in Table 3. To study the relative production of strangeness and compare it with results in pp and Pb–Pb collisions, the yield ratios to pions were calculated as a function of charged particle multiplicity. Both the $(\Xi^- + \Xi^+)/(\pi^+ + \pi^-)$ and $(\Omega^- + \Omega^+)/(\pi^+ + \pi^-)$

ratios are observed to increase as a function of multiplicity, as seen in Fig. 4. The relative increase is more pronounced for the Ω^- and Ω^+ than for Ξ^- and Ξ^+ , being approximately 100% for the former and 60% for the latter. These relative increases are larger than the 30% increase observed for the Λ/π ratio [23], indicating that strangeness content may control the rate of increase with multiplicity.

These ratios are further compared to measurements performed in the pp [25,34] and Pb–Pb [10] collision systems. The $(\Xi^- + \Xi^+)/(\pi^+ + \pi^-)$ ratio for the highest p–Pb multiplicity is compatible with the Pb–Pb measurements in the Pb–Pb 0–60% centrality range and the $(\Omega^- + \Omega^+)/(\pi^+ + \pi^-)$ reaches a value slightly below its Pb–Pb equivalent in this centrality range, although the error bars still overlap. It is also noteworthy that the values obtained for the p–Pb 80–100% multiplicity event class are similar to the ones measured in minimum bias pp collisions.

Finally, the hyperon to pion ratios can also be compared with the values in the Grand Canonical (GC) limit obtained from global fits to Pb–Pb data. Two different implementations of the thermal model are shown in Fig. 4, where the dashed lines represent the values from the THERMUS 2.3 model [36] and the solid lines represent predictions from the GSI–Heidelberg model [35]. Both models provide values that are consistent with the most central Pb–Pb measurements.

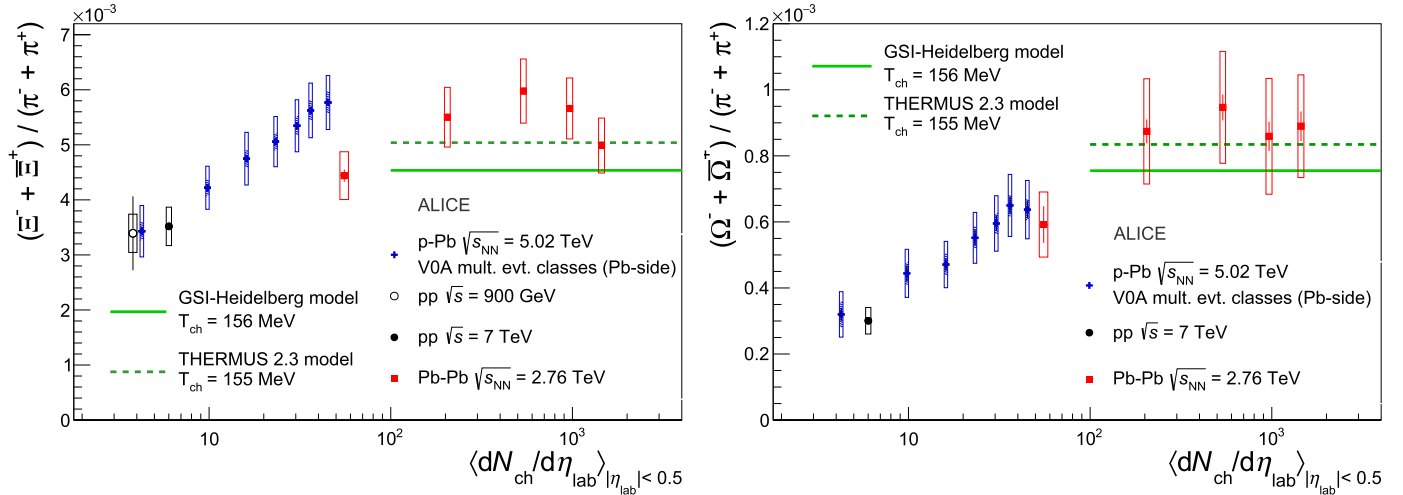


Fig. 4. (Colour online.) $(\Xi^- + \Xi^+) / (\pi^+ + \pi^-)$ (left) and $(\Omega^- + \Omega^+) / (\pi^+ + \pi^-)$ (right) ratios as a function of $\langle dN_{ch}/d\eta \rangle$ for all three colliding systems. The ratios for the seven multiplicity classes in p-Pb data lie between the Minimum Bias pp ($\sqrt{s} = 900$ GeV [32,33] and $\sqrt{s} = 7$ TeV [25,34]) and peripheral Pb-Pb results. The Pb-Pb points [10] represent, from left to right, the 60–80%, 40–60%, 20–40% and 10–20% centrality classes. The chemical equilibrium predictions by the GSI-Heidelberg [35] and the THERMUS 2.3 [36] models are represented by the horizontal lines.

In small multiplicity environments such as those produced in p-Pb collisions, a grand canonical statistical description may not be appropriate. Instead, local conservation laws might play an important role. The evolution of hyperon to pion ratios in terms of the event multiplicity can be calculated with a Strangeness Canonical (SC) model implemented in THERMUS [36]. This model applies a local conservation law to the strangeness quantum number within a correlation volume V_c while treating the baryon and charge quantum numbers grand-canonically within the fireball volume V . This implies a decrease of the strangeness yields with respect to the pion yields with a shrinking system size. To model this canonical suppression effect as a function of pion rapidity density, yield calculations were repeated for varying system sizes. Strangeness conservation was imposed within the size of the fireball ($V_c = V$), and the strangeness saturation parameter γ_s was fixed to 1, thus changes in the hadron to pion ratios were due to the variations of the restraints on the system size only. The chemical potentials (μ) of the conserved strangeness, baryon and electric charge quantum numbers were set to zero. The obtained suppression curves for Λ , Ξ and Ω are shown in Fig. 5 for a temperature of 155 MeV, the value extracted from a GC global fit to high multiplicity Pb-Pb data, with a variation of ± 10 MeV (solid lines). Both the data and model points were normalised to the high multiplicity limit. For the data, this limit is the mean hyperon to pion ratio in the 0–60% most central Pb-Pb events, whereas for the model it corresponds to the GC limit. The theoretical curves for strangeness suppression computed with THERMUS are in qualitative agreement with the effect observed in the data.

4. Conclusions

In summary, a measurement of the p_T spectra of Ξ^- , Ξ^+ , Ω^- and Ω^+ for seven multiplicity classes in p-Pb collisions at $\sqrt{s_{NN}} = 5.02$ TeV at the LHC has been presented. These measurements represent an important contribution to the understanding of strangeness production, as hyperon production rates are now measured at LHC energies over a large range in charged-particle multiplicity, from pp to central Pb-Pb collisions.

The multi-strange baryon spectra exhibit a progressive flattening with increasing multiplicity suggesting the presence of radial

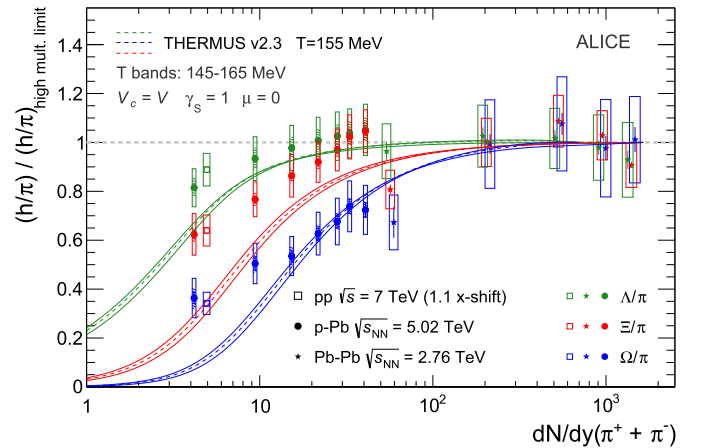


Fig. 5. (Colour online.) Hyperon to pion ratios as a function of pion yields for pp, p-Pb and Pb-Pb colliding systems compared to the THERMUS [36] strangeness suppression model prediction, in which only the system size is varied. The h/π are the ratios of the particle and antiparticle sums, except for the $2\Lambda/(\pi^- + \pi^+)$ data points in pp [33], p-Pb [23] and Pb-Pb [37]. All values are normalised to the high multiplicity limit, which is given by the mean of the 0–60% highest multiplicity Pb-Pb measurements for the data and by the GC limit for the model.

flow. A comparison with the Boltzmann–Gibbs Blast-Wave model indicates a common kinetic freeze-out with lighter hadrons in the highest multiplicity p-Pb collisions. This is in contrast to higher multiplicity heavy-ion collisions where there is an indication for an earlier freeze-out of these particles.

For the first time, the lifting of strangeness suppression with system size has been observed with measurements in a single collision system. Hyperon to pion ratios are shown to increase with multiplicity in p-Pb collisions from the values measured in pp to those observed in Pb-Pb. The rate of increase is more pronounced for particles with higher strangeness content. Comparing these results to the trends observed in statistical hadronisation models that conserve strangeness across the created system indicates that the behaviour is qualitatively consistent with the lifting of canonical suppression with increasing multiplicity.

Acknowledgements

The ALICE Collaboration would like to thank all its engineers and technicians for their invaluable contributions to the construction of the experiment and the CERN accelerator teams for the outstanding performance of the LHC complex. The ALICE Collaboration gratefully acknowledges the resources and support provided by all Grid centres and the Worldwide LHC Computing Grid (WLCG) collaboration. The ALICE Collaboration acknowledges the following funding agencies for their support in building and running the ALICE detector: State Committee of Science, World Federation of Scientists (WFS) and Swiss Fonds Kidagan, Armenia; Conselho Nacional de Desenvolvimento Científico e Tecnológico (CNPq), Financiadora de Estudos e Projetos (FINEP), Fundação de Amparo à Pesquisa do Estado de São Paulo (FAPESP); National Natural Science Foundation of China (NSFC), the Chinese Ministry of Education (CMOE) and the Ministry of Science and Technology of China (MSTC); Ministry of Education and Youth of the Czech Republic; Danish Natural Science Research Council, the Carlsberg Foundation and the Danish National Research Foundation; The European Research Council under the European Community's Seventh Framework Programme; Helsinki Institute of Physics and the Academy of Finland; French CNRS-IN2P3, the 'Region Pays de Loire', 'Region Alsace', 'Region Auvergne' and CEA, France; German Bundesministerium für Bildung, Wissenschaft, Forschung und Technologie (BMBF) and the Helmholtz Association; General Secretariat for Research and Technology, Ministry of Development, Greece; National Research, Development and Innovation Office (NKFIH), Hungary; Department of Atomic Energy and Department of Science and Technology of the Government of India; Istituto Nazionale di Fisica Nucleare (INFN) and Centro Fermi – Museo Storico della Fisica e Centro Studi e Ricerche “Enrico Fermi”, Italy; Japan Society for the Promotion of Science (JSPS) KAKENHI and MEXT, Japan; Joint Institute for Nuclear Research, Dubna; National Research Foundation of Korea (NRF); Consejo Nacional de Ciencia y Tecnología (CONACYT), Dirección General de Asuntos del Personal Académico (DGAPA), México, Amérique Latine Formation académique – European Commission (ALFA-EC) and the EPLANET Program (European Particle Physics Latin American Network); Stichting voor Fundamenteel Onderzoek der Materie (FOM) and the Nederlandse Organisatie voor Wetenschappelijk Onderzoek (NWO), Netherlands; Research Council of Norway (NFR); National Science Centre, Poland; Ministry of National Education/Institute for Atomic Physics and National Council of Scientific Research in Higher Education (CNCSI-UEFISCDI), Romania; Ministry of Education and Science of Russian Federation, Russian Academy of Sciences, Russian Federal Agency of Atomic Energy, Russian Federal Agency for Science and Innovation and The Russian Foundation for Basic Research; Ministry of Education of Slovakia; Department of Science and Technology, Republic of South Africa, South Africa; Centro de Investigaciones Energéticas, Medioambientales y Tecnológicas (CIEMAT), E-Infrastructure shared between Europe and Latin America (EELA), Ministerio de Economía y Competitividad (MINECO) of Spain, Xunta de Galicia (Consellería de Educación), Centro de Aplicaciones Tecnológicas y Desarrollo Nuclear (CEADEN), Cubaenergía, Cuba, and IAEA (International Atomic Energy Agency); Swedish Research Council (VR) and Knut & Alice Wallenberg Foundation (KAW); Ukraine Ministry of Education and Science; United Kingdom Science and Technology Facilities Council (STFC); The United States Department of Energy, the United States National Science Foundation, the State of Texas, and the State of Ohio; Ministry of Science, Education and Sports of Croatia and Unity through Knowledge Fund, Croatia; Council of Scientific and Industrial Research (CSIR), New Delhi, India; Pontificia Universidad Católica del Perú.

References

- [1] J. Rafelski, B. Müller, Strangeness production in the quark–gluon plasma, Phys. Rev. Lett. 48 (1982) 1066–1069, <http://link.aps.org/doi/10.1103/PhysRevLett.48.1066>, Phys. Rev. Lett. 56 (1986) 2334 (Erratum).
- [2] WA97 Collaboration, E. Andersen, et al., Enhancement of central Λ , Ξ and Ω yields in Pb–Pb collisions at 158 A GeV/c, Phys. Lett. B 433 (1998) 209–216, <http://www.sciencedirect.com/science/article/pii/S0370269398006893>.
- [3] WA97 Collaboration, E. Andersen, et al., Strangeness enhancement at mid-rapidity in Pb–Pb collisions at 158 A GeV/c, Phys. Lett. B 449 (1999) 401–406, <http://www.sciencedirect.com/science/article/pii/S0370269399001409>.
- [4] NA49 Collaboration, S. Afanasiev, et al., Ξ^- and Ξ^+ production in central Pb+Pb collisions at 158 GeV/c per nucleon, Phys. Lett. B 538 (2002) 275–281, <http://www.sciencedirect.com/science/article/pii/S0370269302019706>.
- [5] NA57 Collaboration, F. Antinori, et al., Energy dependence of hyperon production in nucleus–nucleus collisions at SPS, Phys. Lett. B 595 (2004) 68–74, <http://www.sciencedirect.com/science/article/pii/S0370269304007725>.
- [6] NA49 Collaboration, T. Anticic, et al., Λ and $\bar{\Lambda}$ production in central Pb–Pb collisions at 40, 80, and 158A GeV, Phys. Rev. Lett. 93 (2004) 022302, <http://link.aps.org/doi/10.1103/PhysRevLett.93.022302>.
- [7] STAR Collaboration, J. Adams, et al., Multistrange baryon production in Au–Au collisions at $\sqrt{s_{NN}} = 130$ GeV, Phys. Rev. Lett. 92 (2004) 182301, <http://link.aps.org/doi/10.1103/PhysRevLett.92.182301>.
- [8] STAR Collaboration, J. Adams, et al., Scaling properties of hyperon production in Au + Au collisions at $\sqrt{s_{NN}} = 200$ GeV, Phys. Rev. Lett. 98 (2007) 062301, <http://link.aps.org/doi/10.1103/PhysRevLett.98.062301>.
- [9] STAR Collaboration, B.I. Abelev, et al., Enhanced strange baryon production in Au+Au collisions compared to p+p at $\sqrt{s_{NN}} = 200$ GeV, Phys. Rev. C 77 (2008) 044908, <http://link.aps.org/doi/10.1103/PhysRevC.77.044908>.
- [10] ALICE Collaboration, B. Abelev, et al., Multi-strange baryon production at mid-rapidity in Pb–Pb collisions at $\sqrt{s_{NN}} = 2.76$ TeV, Phys. Lett. B 728 (2014) 216–227, <http://www.sciencedirect.com/science/article/pii/S0370269313009544>.
- [11] K. Redlich, A. Tounsi, Strangeness enhancement and energy dependence in heavy ion collisions, Eur. Phys. J. C 24 (2002) 589–594, <http://link.springer.com/article/10.1007/s10052-002-0983-1>.
- [12] I. Kraus, J. Cleymans, H. Oeschler, K. Redlich, Particle production in p–p collisions and predictions for $\sqrt{s} = 14$ TeV at the CERN Large Hadron Collider (LHC), Phys. Rev. C 79 (2009) 014901, <http://link.aps.org/doi/10.1103/PhysRevC.79.014901>.
- [13] F. Becattini, J. Manninen, Strangeness production from SPS to LHC, J. Phys. G, Nucl. Part. Phys. 35 (2008) 104013, <http://stacks.iop.org/0954-3899/35/i=10/a=104013>.
- [14] J. Aichelin, K. Werner, Centrality dependence of strangeness enhancement in ultrarelativistic heavy ion collisions: a core-corona effect, Phys. Rev. C 79 (2009) 064907, arXiv:0810.4465 [nucl-th], <http://link.aps.org/doi/10.1103/PhysRevC.79.064907>, Phys. Rev. C 81 (2010) 029902 (Erratum).
- [15] STAR Collaboration, G. Agakishiev, et al., Strangeness enhancement in Cu–Cu and Au–Au collisions at $\sqrt{s_{NN}} = 200$ GeV, Phys. Rev. Lett. 108 (2012) 072301, <http://link.aps.org/doi/10.1103/PhysRevLett.108.072301>.
- [16] E. Schnedermann, J. Sollfrank, U.W. Heinz, Thermal phenomenology of hadrons from 200A GeV S+S collisions, Phys. Rev. C 48 (1993) 2462–2475, arXiv:nucl-th/9307020, <http://link.aps.org/doi/10.1103/PhysRevC.48.2462>.
- [17] V. Begun, W. Florkowski, M. Rybczynski, Transverse-momentum spectra of strange particles produced in Pb + Pb collisions at $\sqrt{s_{NN}} = 2.76$ TeV in the chemical nonequilibrium model, Phys. Rev. C 90 (2014) 054912, <http://link.aps.org/doi/10.1103/PhysRevC.90.054912>.
- [18] I. Melo, B. Tomasik, Blast wave fits with resonances to p_T spectra from nuclear collisions at the LHC, in: 15th International Conference on Strangeness in Quark Matter (SQM 2015) Dubna, Moscow region, Russia, July 6–11, 2015, 2015, arXiv:1509.05383 [nucl-th].
- [19] STAR Collaboration, J. Adams, et al., Experimental and theoretical challenges in the search for the quark–gluon plasma: the STAR Collaboration's critical assessment of the evidence from RHIC collisions, Nucl. Phys. A 757 (2005) 102–183, arXiv:nucl-ex/0501009, <http://www.sciencedirect.com/science/article/pii/S0375947405005294>.
- [20] ALICE Collaboration, The ALICE experiment at the CERN LHC, J. Instrum. 3 (2008) S08002, <http://stacks.iop.org/1748-0221/3/i=08/a=S08002>.
- [21] ALICE Collaboration, Performance of the ALICE VZERO system, J. Instrum. 8 (2013) P10016, <http://stacks.iop.org/1748-0221/8/i=10/a=P10016>.
- [22] ALICE Collaboration, B. Abelev, et al., Pseudorapidity density of charged particles in p + Pb collisions at $\sqrt{s_{NN}} = 5.02$ TeV, Phys. Rev. Lett. 110 (2013) 032301, <http://link.aps.org/doi/10.1103/PhysRevLett.110.032301>.
- [23] ALICE Collaboration, J. Adam, et al., Multiplicity dependence of pion, kaon, proton and lambda production in p–Pb collisions at $\sqrt{s_{NN}} = 5.02$ TeV, Phys. Lett. B 728 (2014) 25–38, <http://www.sciencedirect.com/science/article/pii/S0370269313009234>.

- [24] K.A. Olive, et al., Particle data group, *Chin. Phys. C* 38 (2014) 090001, <http://stacks.iop.org/1674-1137/38/i=9/a=090001>.
- [25] ALICE Collaboration, B. Abelev, et al., Multi-strange baryon production in pp collisions at $\sqrt{s} = 7$ TeV with ALICE, *Phys. Lett. B* 712 (2012) 309–318, <http://www.sciencedirect.com/science/article/pii/S037026931200528X>.
- [26] ALICE Collaboration, Performance of the ALICE experiment at the CERN LHC, *Int. J. Mod. Phys. A* 29 (2014) 1430044, <http://www.worldscientific.com/doi/abs/10.1142/S0217751X14300440>.
- [27] S. Roesler, R. Engel, J. Ranft, The Monte Carlo event generator DPMJET-III, in: A. Kling, F. Barão, M. Nakagawa, L. Távora, P. Vaz (Eds.), *Advanced Monte Carlo for Radiation Physics, Particle Transport Simulation and Applications*, Springer, Berlin, Heidelberg, 2001, pp. 1033–1038, arXiv:hep-ph/0012252.
- [28] R. Brun, F. Bruyant, F. Carminati, S. Giani, M. Maire, A. McPherson, G. Patrick, L. Urban, Geant detector description and simulation tool, CERN Program Library Long Writup (1994).
- [29] C. Tsallis, Possible generalization of Boltzmann–Gibbs statistics, *J. Stat. Phys.* 52 (1988) 479–487.
- [30] T. Sjostrand, S. Mrenna, P.Z. Skands, PYTHIA 6.4 physics and manual, *J. High Energy Phys.* 05 (2006) 026, arXiv:hep-ph/0603175.
- [31] A. Ortiz Velasquez, P. Christiansen, E. Cuautle Flores, I.A. Maldonado Cervantes, G. Paic, Color reconnection and flowlike patterns in pp collisions, *Phys. Rev. Lett.* 111 (2013) 042001, <http://link.aps.org/doi/10.1103/PhysRevLett.111.042001>.
- [32] ALICE Collaboration, K. Aamodt, et al., Production of pions, kaons and protons in pp collisions at $\sqrt{s} = 900$ GeV with ALICE at the LHC, *Eur. Phys. J. C* 71 (2011) 1655, <http://dx.doi.org/10.1140/epjc/s10052-011-1655-9>.
- [33] ALICE Collaboration, K. Aamodt, et al., Strange particle production in proton–proton collisions at $\sqrt{s} = 0.9$ TeV with ALICE at the LHC, *Eur. Phys. J. C* 71 (2011) 1594, <http://dx.doi.org/10.1140/epjc/s10052-011-1594-5>.
- [34] ALICE Collaboration, J. Adam, et al., Measurement of pion, kaon and proton production in proton–proton collisions at $\sqrt{s} = 7$ TeV, *Eur. Phys. J. C* 75 (2015) 226, <http://dx.doi.org/10.1140/epjc/s10052-015-3422-9>.
- [35] A. Andronic, P. Braun-Munzinger, J. Stachel, Thermal hadron production in relativistic nuclear collisions: the hadron mass spectrum, the horn, and the QCD phase transition, *Phys. Lett. B* 673 (2009) 142–145, <http://www.sciencedirect.com/science/article/pii/S0370269309001609>.
- [36] S. Wheaton, J. Cleymans, M. Hauer, THERMUS – a thermal model package for ROOT, *Comput. Phys. Commun.* 180 (2009) 84–106, <http://www.sciencedirect.com/science/article/pii/S0010465508002750>.
- [37] ALICE Collaboration, B.B. Abelev, et al., K_S^0 and Λ production in Pb–Pb collisions at $\sqrt{s_{NN}} = 2.76$ TeV, *Phys. Rev. Lett.* 111 (2013) 222301, arXiv:1307.5530 [nucl-ex].

ALICE Collaboration

J. Adam⁴⁰, D. Adamová⁸⁴, M.M. Aggarwal⁸⁸, G. Aglieri Rinella³⁶, M. Agnello¹¹⁰, N. Agrawal⁴⁸, Z. Ahammed¹³², S. Ahmad¹⁹, S.U. Ahn⁶⁸, S. Aiola¹³⁶, A. Akindinov⁵⁸, S.N. Alam¹³², D. Aleksandrov⁸⁰, B. Alessandro¹¹⁰, D. Alexandre¹⁰¹, R. Alfaro Molina⁶⁴, A. Alici^{12,104}, A. Alkin³, J.R.M. Almaraz¹¹⁹, J. Alme³⁸, T. Alt⁴³, S. Altinpinar¹⁸, I. Altsybeev¹³¹, C. Alves Garcia Prado¹²⁰, C. Andrei⁷⁸, A. Andronic⁹⁷, V. Anguelov⁹⁴, J. Anielski⁵⁴, T. Antičić⁹⁸, F. Antinori¹⁰⁷, P. Antonioli¹⁰⁴, L. Aphecetche¹¹³, H. Appelshäuser⁵³, S. Arcelli²⁸, R. Arnaldi¹¹⁰, O.W. Arnold^{37,93}, I.C. Arsene²², M. Arslanok⁵³, B. Audurier¹¹³, A. Augustinus³⁶, R. Averbeck⁹⁷, M.D. Azmi¹⁹, A. Badalà¹⁰⁶, Y.W. Baek⁶⁷, S. Bagnasco¹¹⁰, R. Bailhache⁵³, R. Bala⁹¹, S. Balasubramanian¹³⁶, A. Baldisseri¹⁵, R.C. Baral⁶¹, A.M. Barbano²⁷, R. Barbera²⁹, F. Barile³³, G.G. Barnaföldi¹³⁵, L.S. Barnby¹⁰¹, V. Barret⁷⁰, P. Bartalini⁷, K. Barth³⁶, J. Bartke¹¹⁷, E. Bartsch⁵³, M. Basile²⁸, N. Bastid⁷⁰, S. Basu¹³², B. Bathen⁵⁴, G. Batigne¹¹³, A. Batista Camejo⁷⁰, B. Batyunya⁶⁶, P.C. Batzing²², I.G. Bearden⁸¹, H. Beck⁵³, C. Bedda¹¹⁰, N.K. Behera⁵⁰, I. Belikov⁵⁵, F. Bellini²⁸, H. Bello Martinez², R. Bellwied¹²², R. Belmont¹³⁴, E. Belmont-Moreno⁶⁴, V. Belyaev⁷⁵, P. Benacek⁸⁴, G. Bencedi¹³⁵, S. Beole²⁷, I. Berceanu⁷⁸, A. Bercuci⁷⁸, Y. Berdnikov⁸⁶, D. Berenyi¹³⁵, R.A. Bertens⁵⁷, D. Berzano³⁶, L. Betev³⁶, A. Bhasin⁹¹, I.R. Bhat⁹¹, A.K. Bhati⁸⁸, B. Bhattacharjee⁴⁵, J. Bhom¹²⁸, L. Bianchi¹²², N. Bianchi⁷², C. Bianchin^{134,57}, J. Bielčik⁴⁰, J. Bielčíková⁸⁴, A. Bilandzic^{81,37,93}, G. Biro¹³⁵, R. Biswas⁴, S. Biswas⁷⁹, S. Bjelogrić⁵⁷, J.T. Blair¹¹⁸, D. Blau⁸⁰, C. Blume⁵³, F. Bock^{74,94}, A. Bogdanov⁷⁵, H. Bøggild⁸¹, L. Boldizsár¹³⁵, M. Bombara⁴¹, J. Book⁵³, H. Borel¹⁵, A. Borissov⁹⁶, M. Borri^{83,124}, F. Bossú⁶⁵, E. Botta²⁷, C. Bourjau⁸¹, P. Braun-Munzinger⁹⁷, M. Bregant¹²⁰, T. Breitner⁵², T.A. Broker⁵³, T.A. Browning⁹⁵, M. Broz⁴⁰, E.J. Brucken⁴⁶, E. Bruna¹¹⁰, G.E. Bruno³³, D. Budnikov⁹⁹, H. Buesching⁵³, S. Bufalino^{36,27}, P. Buncic³⁶, O. Busch^{94,128}, Z. Buthelezi⁶⁵, J.B. Butt¹⁶, J.T. Buxton²⁰, D. Caffarri³⁶, X. Cai⁷, H. Caines¹³⁶, L. Calero Diaz⁷², A. Caliva⁵⁷, E. Calvo Villar¹⁰², P. Camerini²⁶, F. Carena³⁶, W. Carena³⁶, F. Carnesecchi²⁸, J. Castillo Castellanos¹⁵, A.J. Castro¹²⁵, E.A.R. Casula²⁵, C. Ceballos Sanchez⁹, P. Cerello¹¹⁰, J. Cerkala¹¹⁵, B. Chang¹²³, S. Chapeland³⁶, M. Chartier¹²⁴, J.L. Charvet¹⁵, S. Chattopadhyay¹³², S. Chattopadhyay¹⁰⁰, A. Chauvin^{93,37}, V. Chelnokov³, M. Cherney⁸⁷, C. Cheshkov¹³⁰, B. Cheynis¹³⁰, V. Chibante Barroso³⁶, D.D. Chinellato¹²¹, S. Cho⁵⁰, P. Chochula³⁶, K. Choi⁹⁶, M. Chojnacki⁸¹, S. Choudhury¹³², P. Christakoglou⁸², C.H. Christensen⁸¹, P. Christiansen³⁴, T. Chujo¹²⁸, S.U. Chung⁹⁶, C. Cicalo¹⁰⁵, L. Cifarelli^{12,28}, F. Cindolo¹⁰⁴, J. Cleymans⁹⁰, F. Colamaria³³, D. Colella^{59,36}, A. Collu^{74,25}, M. Colocci²⁸, G. Conesa Balbastre⁷¹, Z. Conesa del Valle⁵¹, M.E. Connors^{136,ii}, J.G. Contreras⁴⁰, T.M. Cormier⁸⁵, Y. Corrales Morales¹¹⁰, I. Cortés Maldonado², P. Cortese³², M.R. Cosentino¹²⁰, F. Costa³⁶, P. Crochet⁷⁰, R. Cruz Albino¹¹, E. Cuautle⁶³, L. Cunqueiro^{54,36}, T. Dahms^{93,37}, A. Dainese¹⁰⁷, A. Danu⁶², D. Das¹⁰⁰, I. Das^{100,51}, S. Das⁴, A. Dash^{121,79}, S. Dash⁴⁸, S. De¹²⁰, A. De Caro^{12,31}, G. de Cataldo¹⁰³, C. de Conti¹²⁰, J. de Cuveland⁴³, A. De Falco²⁵, D. De Gruttola^{12,31}, N. De Marco¹¹⁰, S. De Pasquale³¹, A. Deisting^{97,94}, A. Deloff⁷⁷, E. Dénes^{135,i}, C. Deplano⁸², P. Dhanukher⁴⁸, D. Di Bari³³, A. Di Mauro³⁶, P. Di Nezza⁷², M.A. Diaz Corchero¹⁰, T. Dietel⁹⁰, P. Dillenseger⁵³, R. Divià³⁶, Ø. Djuvsland¹⁸, A. Dobrin^{57,82},

D. Domenicis Gimenez ¹²⁰, B. Dönigus ⁵³, O. Dordic ²², T. Drozhzhova ⁵³, A.K. Dubey ¹³², A. Dubla ⁵⁷,
 L. Ducroux ¹³⁰, P. Dupieux ⁷⁰, R.J. Ehlers ¹³⁶, D. Elia ¹⁰³, E. Endress ¹⁰², H. Engel ⁵², E. Eppele ¹³⁶,
 B. Erazmus ¹¹³, I. Erdemir ⁵³, F. Erhardt ¹²⁹, B. Espagnon ⁵¹, M. Estienne ¹¹³, S. Esumi ¹²⁸, J. Eum ⁹⁶,
 D. Evans ¹⁰¹, S. Evdokimov ¹¹¹, G. Eyyubova ⁴⁰, L. Fabbietti ^{93,37}, D. Fabris ¹⁰⁷, J. Faivre ⁷¹, A. Fantoni ⁷²,
 M. Fasel ⁷⁴, L. Feldkamp ⁵⁴, A. Feliciello ¹¹⁰, G. Feofilov ¹³¹, J. Ferencei ⁸⁴, A. Fernández Téllez ²,
 E.G. Ferreira ¹⁷, A. Ferretti ²⁷, A. Festanti ³⁰, V.J.G. Feuillard ^{15,70}, J. Figiel ¹¹⁷, M.A.S. Figueredo ^{124,120},
 S. Filchagin ⁹⁹, D. Finogeev ⁵⁶, F.M. Fionda ²⁵, E.M. Fiore ³³, M.G. Fleck ⁹⁴, M. Floris ³⁶, S. Foertsch ⁶⁵,
 P. Foka ⁹⁷, S. Fokin ⁸⁰, E. Fragiaco ¹⁰⁹, A. Francescon ^{36,30}, U. Frankenfeld ⁹⁷, G.G. Fronze ²⁷, U. Fuchs ³⁶,
 C. Furget ⁷¹, A. Furs ⁵⁶, M. Fusco Girard ³¹, J.J. Gaardhøje ⁸¹, M. Gagliardi ²⁷, A.M. Gago ¹⁰², M. Gallio ²⁷,
 D.R. Gangadharan ⁷⁴, P. Ganoti ⁸⁹, C. Gao ⁷, C. Garabatos ⁹⁷, E. Garcia-Solis ¹³, C. Gargiulo ³⁶, P. Gasik ^{93,37},
 E.F. Gauger ¹¹⁸, M. Germain ¹¹³, A. Gheata ³⁶, M. Gheata ^{36,62}, P. Ghosh ¹³², S.K. Ghosh ⁴, P. Gianotti ⁷²,
 P. Giubellino ^{110,36}, P. Giubilato ³⁰, E. Gladysz-Dziadus ¹¹⁷, P. Glässel ⁹⁴, D.M. Gómez Coral ⁶⁴,
 A. Gomez Ramirez ⁵², V. Gonzalez ¹⁰, P. González-Zamora ¹⁰, S. Gorbunov ⁴³, L. Görlich ¹¹⁷, S. Gotovac ¹¹⁶,
 V. Grabski ⁶⁴, O.A. Grachov ¹³⁶, L.K. Graczykowski ¹³³, K.L. Graham ¹⁰¹, A. Grelli ⁵⁷, A. Grigoras ³⁶,
 C. Grigoras ³⁶, V. Grigoriev ⁷⁵, A. Grigoryan ¹, S. Grigoryan ⁶⁶, B. Grinyov ³, N. Grion ¹⁰⁹, J.M. Gronefeld ⁹⁷,
 J.F. Grosse-Oetringhaus ³⁶, J.-Y. Grossiord ¹³⁰, R. Grosso ⁹⁷, F. Guber ⁵⁶, R. Guernane ⁷¹, B. Guerzoni ²⁸,
 K. Gulbrandsen ⁸¹, T. Gunji ¹²⁷, A. Gupta ⁹¹, R. Gupta ⁹¹, R. Haake ⁵⁴, Ø. Haaland ¹⁸, C. Hadjidakis ⁵¹,
 M. Haiduc ⁶², H. Hamagaki ¹²⁷, G. Hamar ¹³⁵, J.C. Hamon ⁵⁵, J.W. Harris ¹³⁶, A. Harton ¹³,
 D. Hatzifotiadou ¹⁰⁴, S. Hayashi ¹²⁷, S.T. Heckel ⁵³, H. Helstrup ³⁸, A. Herghelegiu ⁷⁸, G. Herrera Corral ¹¹,
 B.A. Hess ³⁵, K.F. Hetland ³⁸, H. Hillemanns ³⁶, B. Hippolyte ⁵⁵, D. Horak ⁴⁰, R. Hosokawa ¹²⁸, P. Hristov ³⁶,
 M. Huang ¹⁸, T.J. Humanic ²⁰, N. Hussain ⁴⁵, T. Hussain ¹⁹, D. Hutter ⁴³, D.S. Hwang ²¹, R. Ilkaev ⁹⁹,
 M. Inaba ¹²⁸, E. Incani ²⁵, M. Ippolitov ^{75,80}, M. Irfan ¹⁹, M. Ivanov ⁹⁷, V. Ivanov ⁸⁶, V. Izucheev ¹¹¹,
 N. Jacazio ²⁸, P.M. Jacobs ⁷⁴, M.B. Jadhav ⁴⁸, S. Jadlovská ¹¹⁵, J. Jadlovsky ^{115,59}, C. Jahnke ¹²⁰,
 M.J. Jakubowska ¹³³, H.J. Jang ⁶⁸, M.A. Janik ¹³³, P.H.S.Y. Jayarathna ¹²², C. Jena ³⁰, S. Jena ¹²²,
 R.T. Jimenez Bustamante ⁹⁷, P.G. Jones ¹⁰¹, H. Jung ⁴⁴, A. Jusko ¹⁰¹, P. Kalinak ⁵⁹, A. Kalweit ³⁶, J. Kamin ⁵³,
 J.H. Kang ¹³⁷, V. Kaplin ⁷⁵, S. Kar ¹³², A. Karasu Uysal ⁶⁹, O. Karavichev ⁵⁶, T. Karavicheva ⁵⁶,
 L. Karayan ^{97,94}, E. Karpechev ⁵⁶, U. Keschull ⁵², R. Keidel ¹³⁸, D.L.D. Keijdener ⁵⁷, M. Keil ³⁶,
 M. Mohisin Khan ^{19,iii}, P. Khan ¹⁰⁰, S.A. Khan ¹³², A. Khanzadeev ⁸⁶, Y. Kharlov ¹¹¹, B. Kileng ³⁸,
 D.W. Kim ⁴⁴, D.J. Kim ¹²³, D. Kim ¹³⁷, H. Kim ¹³⁷, J.S. Kim ⁴⁴, M. Kim ⁴⁴, M. Kim ¹³⁷, S. Kim ²¹, T. Kim ¹³⁷,
 S. Kirsch ⁴³, I. Kisel ⁴³, S. Kiselev ⁵⁸, A. Kisiel ¹³³, G. Kiss ¹³⁵, J.L. Klay ⁶, C. Klein ⁵³, J. Klein ³⁶,
 C. Klein-Bösing ⁵⁴, S. Klewin ⁹⁴, A. Kluge ³⁶, M.L. Knichel ⁹⁴, A.G. Knospe ¹¹⁸, C. Kobdaj ¹¹⁴, M. Kofarago ³⁶,
 T. Kollegger ⁹⁷, A. Kolojvari ¹³¹, V. Kondratiev ¹³¹, N. Kondratyeva ⁷⁵, E. Kondratyuk ¹¹¹, A. Konevskikh ⁵⁶,
 M. Kopicik ¹¹⁵, M. Kour ⁹¹, C. Kouzinopoulos ³⁶, O. Kovalenko ⁷⁷, V. Kovalenko ¹³¹, M. Kowalski ¹¹⁷,
 G. Koyithatta Meethalevedu ⁴⁸, I. Králik ⁵⁹, A. Kravčáková ⁴¹, M. Kretz ⁴³, M. Krivda ^{59,101}, F. Krizek ⁸⁴,
 E. Kryshen ^{86,36}, M. Krzewicki ⁴³, A.M. Kubera ²⁰, V. Kučera ⁸⁴, C. Kuhn ⁵⁵, P.G. Kuijper ⁸², A. Kumar ⁹¹,
 J. Kumar ⁴⁸, L. Kumar ⁸⁸, S. Kumar ⁴⁸, P. Kurashvili ⁷⁷, A. Kurepin ⁵⁶, A.B. Kurepin ⁵⁶, A. Kuryakin ⁹⁹,
 M.J. Kweon ⁵⁰, Y. Kwon ¹³⁷, S.L. La Pointe ¹¹⁰, P. La Rocca ²⁹, P. Ladrón de Guevara ¹¹,
 C. Lagana Fernandes ¹²⁰, I. Lakomov ³⁶, R. Langoy ⁴², C. Lara ⁵², A. Lardeux ¹⁵, A. Lattuca ²⁷, E. Laudi ³⁶,
 R. Lea ²⁶, L. Leardini ⁹⁴, G.R. Lee ¹⁰¹, S. Lee ¹³⁷, F. Lehas ⁸², R.C. Lemmon ⁸³, V. Lenti ¹⁰³, E. Leogrande ⁵⁷,
 I. León Monzón ¹¹⁹, H. León Vargas ⁶⁴, M. Leoncino ²⁷, P. Lévai ¹³⁵, S. Li ^{7,70}, X. Li ¹⁴, J. Lien ⁴²,
 R. Lietava ¹⁰¹, S. Lindal ²², V. Lindenstruth ⁴³, C. Lippmann ⁹⁷, M.A. Lisa ²⁰, H.M. Ljunggren ³⁴,
 D.F. Lodato ⁵⁷, P.I. Loenne ¹⁸, V. Loginov ⁷⁵, C. Loizides ⁷⁴, X. Lopez ⁷⁰, E. López Torres ⁹, A. Lowe ¹³⁵,
 P. Luettig ⁵³, M. Lunardon ³⁰, G. Luparello ²⁶, T.H. Lutz ¹³⁶, A. Maevskaya ⁵⁶, M. Mager ³⁶, S. Mahajan ⁹¹,
 S.M. Mahmood ²², A. Maire ⁵⁵, R.D. Majka ¹³⁶, M. Malaev ⁸⁶, I. Maldonado Cervantes ⁶³, L. Malinina ^{66,iv},
 D. Mal'Kevich ⁵⁸, P. Malzacher ⁹⁷, A. Mamonov ⁹⁹, V. Manko ⁸⁰, F. Manso ⁷⁰, V. Manzari ^{36,103},
 M. Marchisone ^{65,126,27}, J. Mareš ⁶⁰, G.V. Margagliotti ²⁶, A. Margotti ¹⁰⁴, J. Margutti ⁵⁷, A. Marín ⁹⁷,
 C. Markert ¹¹⁸, M. Marquard ⁵³, N.A. Martin ⁹⁷, J. Martin Blanco ¹¹³, P. Martinengo ³⁶, M.I. Martínez ²,
 G. Martínez García ¹¹³, M. Martinez Pedreira ³⁶, A. Mas ¹²⁰, S. Masciocchi ⁹⁷, M. Maserà ²⁷, A. Masoni ¹⁰⁵,
 L. Massacrier ¹¹³, A. Mastroserio ³³, A. Matyja ¹¹⁷, C. Mayer ^{36,117}, J. Mazer ¹²⁵, M.A. Mazzone ¹⁰⁸,
 D. McDonald ¹²², F. Meddi ²⁴, Y. Melikyan ⁷⁵, A. Menchaca-Rocha ⁶⁴, E. Meninno ³¹, J. Mercado Pérez ⁹⁴,
 M. Meres ³⁹, Y. Miake ¹²⁸, M.M. Mieskolainen ⁴⁶, K. Mikhaylov ^{66,58}, L. Milano ^{74,36}, J. Milosevic ²²,
 L.M. Minervini ^{103,23}, A. Mischke ⁵⁷, A.N. Mishra ⁴⁹, D. Miśkowiec ⁹⁷, J. Mitra ¹³², C.M. Mitu ⁶²,

N. Mohammadi⁵⁷, B. Mohanty^{79,132}, L. Molnar^{55,113}, L. Montaño Zetina¹¹, E. Montes¹⁰,
 D.A. Moreira De Godoy^{54,113}, L.A.P. Moreno², S. Moretto³⁰, A. Morreale¹¹³, A. Morsch³⁶,
 V. Muccifora⁷², E. Mudnic¹¹⁶, D. Mühlheim⁵⁴, S. Muhuri¹³², M. Mukherjee¹³², J.D. Mulligan¹³⁶,
 M.G. Munhoz¹²⁰, R.H. Munzer^{93,37}, H. Murakami¹²⁷, S. Murray⁶⁵, L. Musa³⁶, J. Musinsky⁵⁹, B. Naik⁴⁸,
 R. Nair⁷⁷, B.K. Nandi⁴⁸, R. Nania¹⁰⁴, E. Nappi¹⁰³, M.U. Naru¹⁶, H. Natal da Luz¹²⁰, C. Nattrass¹²⁵,
 S.R. Navarro², K. Nayak⁷⁹, R. Nayak⁴⁸, T.K. Nayak¹³², S. Nazarenko⁹⁹, A. Nedosekin⁵⁸, L. Nellen⁶³,
 F. Ng¹²², M. Nicassio⁹⁷, M. Niculescu⁶², J. Niedziela³⁶, B.S. Nielsen⁸¹, S. Nikolaev⁸⁰, S. Nikulin⁸⁰,
 V. Nikulin⁸⁶, F. Noferini^{104,12}, P. Nomokonov⁶⁶, G. Nooren⁵⁷, J.C.C. Noris², J. Norman¹²⁴, A. Nyanin⁸⁰,
 J. Nystrand¹⁸, H. Oeschler⁹⁴, S. Oh¹³⁶, S.K. Oh⁶⁷, A. Ohlson³⁶, A. Okatan⁶⁹, T. Okubo⁴⁷, L. Olah¹³⁵,
 J. Oleniacz¹³³, A.C. Oliveira Da Silva¹²⁰, M.H. Oliver¹³⁶, J. Onderwaater⁹⁷, C. Oppedisano¹¹⁰, R. Orava⁴⁶,
 A. Ortiz Velasquez⁶³, A. Oskarsson³⁴, J. Otwinowski¹¹⁷, K. Oyama^{94,76}, M. Ozdemir⁵³, Y. Pachmayer⁹⁴,
 P. Pagano³¹, G. Paic⁶³, S.K. Pal¹³², J. Pan¹³⁴, A.K. Pandey⁴⁸, P. Papcun¹¹⁵, V. Papikyan¹,
 G.S. Pappalardo¹⁰⁶, P. Pareek⁴⁹, W.J. Park⁹⁷, S. Parmar⁸⁸, A. Passfeld⁵⁴, V. Paticchio¹⁰³, R.N. Patra¹³²,
 B. Paul¹⁰⁰, H. Pei⁷, T. Peitzmann⁵⁷, H. Pereira Da Costa¹⁵, D. Peresunko^{80,75}, C.E. Pérez Lara⁸²,
 E. Perez Lezama⁵³, V. Peskov⁵³, Y. Pestov⁵, V. Petráček⁴⁰, V. Petrov¹¹¹, M. Petrovici⁷⁸, C. Petta²⁹,
 S. Piano¹⁰⁹, M. Pikna³⁹, P. Pillot¹¹³, L.O.D.L. Pimentel⁸¹, O. Pinazza^{36,104}, L. Pinsky¹²²,
 D.B. Piyarathna¹²², M. Płoskoń⁷⁴, M. Planinic¹²⁹, J. Pluta¹³³, S. Pochybova¹³⁵, P.L.M. Podesta-Lerma¹¹⁹,
 M.G. Poghosyan^{85,87}, B. Polichtchouk¹¹¹, N. Poljak¹²⁹, W. Poonsawat¹¹⁴, A. Pop⁷⁸,
 S. Porteboeuf-Houssais⁷⁰, J. Porter⁷⁴, J. Pospisil⁸⁴, S.K. Prasad⁴, R. Preghenella^{104,36}, F. Prino¹¹⁰,
 C.A. Pruneau¹³⁴, I. Pshenichnov⁵⁶, M. Puccio²⁷, G. Puudu²⁵, P. Pujahari¹³⁴, V. Punin⁹⁹, J. Putschke¹³⁴,
 H. Qvigstad²², A. Rachevski¹⁰⁹, S. Raha⁴, S. Rajput⁹¹, J. Rak¹²³, A. Rakotozafindrabe¹⁵, L. Ramello³²,
 F. Rami⁵⁵, R. Raniwala⁹², S. Raniwala⁹², S.S. Räsänen⁴⁶, B.T. Rascanu⁵³, D. Rathee⁸⁸, K.F. Read^{125,85},
 K. Redlich⁷⁷, R.J. Reed¹³⁴, A. Rehman¹⁸, P. Reichelt⁵³, F. Reidt^{94,36}, X. Ren⁷, R. Renfordt⁵³,
 A.R. Reolon⁷², A. Reshetin⁵⁶, J.-P. Revol¹², K. Reygers⁹⁴, V. Riabov⁸⁶, R.A. Ricci⁷³, T. Richert³⁴,
 M. Richter²², P. Riedler³⁶, W. Riegler³⁶, F. Riggi²⁹, C. Ristea⁶², E. Rocco⁵⁷, M. Rodríguez Cahuantzi^{2,11},
 A. Rodríguez Manso⁸², K. Røed²², E. Rogochaya⁶⁶, D. Rohr⁴³, D. Röhrich¹⁸, R. Romita¹²⁴,
 F. Ronchetti^{72,36}, L. Ronflette¹¹³, P. Rosnet⁷⁰, A. Rossi^{30,36}, F. Roukoutakis⁸⁹, A. Roy⁴⁹, C. Roy⁵⁵,
 P. Roy¹⁰⁰, A.J. Rubio Montero¹⁰, R. Rui²⁶, R. Russo²⁷, E. Ryabinkin⁸⁰, Y. Ryabov⁸⁶, A. Rybicki¹¹⁷,
 S. Sadovsky¹¹¹, K. Šafařík³⁶, B. Sahlmuller⁵³, P. Sahoo⁴⁹, R. Sahoo⁴⁹, S. Sahoo⁶¹, P.K. Sahu⁶¹, J. Saini¹³²,
 S. Sakai⁷², M.A. Saleh¹³⁴, J. Salzwedel²⁰, S. Sambyal⁹¹, V. Samsonov⁸⁶, L. Šándor⁵⁹, A. Sandoval⁶⁴,
 M. Sano¹²⁸, D. Sarkar¹³², P. Sarma⁴⁵, E. Scapparone¹⁰⁴, F. Scarlassara³⁰, C. Schiaua⁷⁸, R. Schicker⁹⁴,
 C. Schmidt⁹⁷, H.R. Schmidt³⁵, S. Schuchmann⁵³, J. Schukraft³⁶, M. Schulc⁴⁰, T. Schuster¹³⁶,
 Y. Schutz^{36,113}, K. Schwarz⁹⁷, K. Schweda⁹⁷, G. Scioli²⁸, E. Scomparin¹¹⁰, R. Scott¹²⁵, M. Šefčík⁴¹,
 J.E. Seger⁸⁷, Y. Sekiguchi¹²⁷, D. Sekihata⁴⁷, I. Selyuzhenkov⁹⁷, K. Senosi⁶⁵, S. Senyukov^{3,36},
 E. Serradilla^{10,64}, A. Sevcenco⁶², A. Shabanov⁵⁶, A. Shabetai¹¹³, O. Shadura³, R. Shahoyan³⁶,
 A. Shangaraev¹¹¹, A. Sharma⁹¹, M. Sharma⁹¹, M. Sharma⁹¹, N. Sharma¹²⁵, K. Shigaki⁴⁷, K. Shtejer^{9,27},
 Y. Sibirak⁸⁰, S. Siddhanta¹⁰⁵, K.M. Sielewicz³⁶, T. Siemiarczuk⁷⁷, D. Silvermyr³⁴, C. Silvestre⁷¹,
 G. Simatovic¹²⁹, G. Simonetti³⁶, R. Singaraju¹³², R. Singh⁷⁹, S. Singha^{132,79}, V. Singhal¹³², B.C. Sinha¹³²,
 T. Sinha¹⁰⁰, B. Sitar³⁹, M. Sitta³², T.B. Skaali²², M. Slupecki¹²³, N. Smirnov¹³⁶, R.J.M. Snellings⁵⁷,
 T.W. Snellman¹²³, C. Søgaard³⁴, J. Song⁹⁶, M. Song¹³⁷, Z. Song⁷, F. Soramel³⁰, S. Sorensen¹²⁵,
 R.D. de Souza¹²¹, F. Sozzi⁹⁷, M. Spacek⁴⁰, E. Spiriti⁷², I. Sputowska¹¹⁷, M. Spyropoulou-Stassinaki⁸⁹,
 J. Stachel⁹⁴, I. Stan⁶², P. Stankus⁸⁵, G. Stefanek⁷⁷, E. Stenlund³⁴, G. Steyn⁶⁵, J.H. Stiller⁹⁴, D. Stocco¹¹³,
 P. Strmen³⁹, A.A.P. Suaide¹²⁰, T. Sugitate⁴⁷, C. Suire⁵¹, M. Suleymanov¹⁶, M. Suljic^{26,1}, R. Sultanov⁵⁸,
 M. Šumbera⁸⁴, A. Szabo³⁹, A. Szanto de Toledo^{120,1}, I. Szarka³⁹, A. Szczepankiewicz³⁶,
 M. Szymanski¹³³, U. Tabassam¹⁶, J. Takahashi¹²¹, G.J. Tambave¹⁸, N. Tanaka¹²⁸, M.A. Tangaro³³,
 M. Tarhini⁵¹, M. Tariq¹⁹, M.G. Tarzila⁷⁸, A. Tauro³⁶, G. Tejeda Muñoz², A. Telesca³⁶, K. Terasaki¹²⁷,
 C. Terrevoli³⁰, B. Teyssier¹³⁰, J. Thäder⁷⁴, D. Thomas¹¹⁸, R. Tieulent¹³⁰, A.R. Timmins¹²², A. Toia⁵³,
 S. Trogolo²⁷, G. Trombetta³³, V. Trubnikov³, W.H. Trzaska¹²³, T. Tsuji¹²⁷, A. Tumkin⁹⁹, R. Turrisi¹⁰⁷,
 T.S. Tveter²², K. Ullaland¹⁸, A. Uras¹³⁰, G.L. Usai²⁵, A. Utrobicic¹²⁹, M. Vajzer⁸⁴, M. Vala⁵⁹,
 L. Valencia Palomo⁷⁰, S. Vallero²⁷, J. Van Der Maarel⁵⁷, J.W. Van Hoorne³⁶, M. van Leeuwen⁵⁷,
 T. Vanat⁸⁴, P. Vande Vyvre³⁶, D. Varga¹³⁵, A. Vargas², M. Vargyas¹²³, R. Varma⁴⁸, M. Vasileiou⁸⁹,
 A. Vasiliev⁸⁰, A. Vauthier⁷¹, V. Vechnin¹³¹, A.M. Veen⁵⁷, M. Veldhoen⁵⁷, A. Velure¹⁸,

M. Venaruzzo⁷³, E. Vercellin²⁷, S. Vergara Limón², R. Vernet⁸, M. Verweij¹³⁴, L. Vickovic¹¹⁶, G. Viesti^{30,i}, J. Viinikainen¹²³, Z. Vilakazi¹²⁶, O. Villalobos Baillie¹⁰¹, A. Villatoro Tello², A. Vinogradov⁸⁰, L. Vinogradov¹³¹, Y. Vinogradov^{99,i}, T. Virgili³¹, V. Vislavicius³⁴, Y.P. Viyogi¹³², A. Vodopyanov⁶⁶, M.A. Völkl⁹⁴, K. Voloshin⁵⁸, S.A. Voloshin¹³⁴, G. Volpe¹³⁵, B. von Haller³⁶, I. Vorobyev^{37,93}, D. Vranic^{97,36}, J. Vrláková⁴¹, B. Vulpescu⁷⁰, B. Wagner¹⁸, J. Wagner⁹⁷, H. Wang⁵⁷, M. Wang^{7,113}, D. Watanabe¹²⁸, Y. Watanabe¹²⁷, M. Weber^{36,112}, S.G. Weber⁹⁷, D.F. Weiser⁹⁴, J.P. Wessels⁵⁴, U. Westerhoff⁵⁴, A.M. Whitehead⁹⁰, J. Wiechula³⁵, J. Wikne²², M. Wilde⁵⁴, G. Wilk⁷⁷, J. Wilkinson⁹⁴, M.C.S. Williams¹⁰⁴, B. Windelband⁹⁴, M. Winn⁹⁴, C.G. Yaldo¹³⁴, H. Yang⁵⁷, P. Yang⁷, S. Yano⁴⁷, C. Yasar⁶⁹, Z. Yin⁷, H. Yokoyama¹²⁸, I.-K. Yoo⁹⁶, J.H. Yoon⁵⁰, V. Yurchenko³, I. Yushmanov⁸⁰, A. Zaborowska¹³³, V. Zaccolo⁸¹, A. Zaman¹⁶, C. Zampolli¹⁰⁴, H.J.C. Zanoli¹²⁰, S. Zaporozhets⁶⁶, N. Zardoshti¹⁰¹, A. Zarochentsev¹³¹, P. Závada⁶⁰, N. Zaviyalov⁹⁹, H. Zbroszczyk¹³³, I.S. Zgura⁶², M. Zhalov⁸⁶, H. Zhang¹⁸, X. Zhang⁷⁴, Y. Zhang⁷, C. Zhang⁵⁷, Z. Zhang⁷, C. Zhao²², N. Zhigareva⁵⁸, D. Zhou⁷, Y. Zhou⁸¹, Z. Zhou¹⁸, H. Zhu¹⁸, J. Zhu^{113,7}, A. Zichichi^{28,12}, A. Zimmermann⁹⁴, M.B. Zimmermann^{54,36}, G. Zinovjev³, M. Zyzak⁴³

¹ A.I. Alikhanyan National Science Laboratory (Yerevan Physics Institute) Foundation, Yerevan, Armenia

² Benemérita Universidad Autónoma de Puebla, Puebla, Mexico

³ Bogolyubov Institute for Theoretical Physics, Kiev, Ukraine

⁴ Bose Institute, Department of Physics and Centre for Astroparticle Physics and Space Science (CAPSS), Kolkata, India

⁵ Budker Institute for Nuclear Physics, Novosibirsk, Russia

⁶ California Polytechnic State University, San Luis Obispo, CA, United States

⁷ Central China Normal University, Wuhan, China

⁸ Centre de Calcul de l'IN2P3, Villeurbanne, France

⁹ Centro de Aplicaciones Tecnológicas y Desarrollo Nuclear (CEADEN), Havana, Cuba

¹⁰ Centro de Investigaciones Energéticas Medioambientales y Tecnológicas (CIEMAT), Madrid, Spain

¹¹ Centro de Investigación y de Estudios Avanzados (CINVESTAV), Mexico City and Mérida, Mexico

¹² Centro Fermi – Museo Storico della Fisica e Centro Studi e Ricerche “Enrico Fermi”, Rome, Italy

¹³ Chicago State University, Chicago, IL, USA

¹⁴ China Institute of Atomic Energy, Beijing, China

¹⁵ Commissariat à l’Energie Atomique, IRFU, Saclay, France

¹⁶ COMSATS Institute of Information Technology (CIIT), Islamabad, Pakistan

¹⁷ Departamento de Física de Partículas and IGFAE, Universidad de Santiago de Compostela, Santiago de Compostela, Spain

¹⁸ Department of Physics and Technology, University of Bergen, Bergen, Norway

¹⁹ Department of Physics, Aligarh Muslim University, Aligarh, India

²⁰ Department of Physics, Ohio State University, Columbus, OH, United States

²¹ Department of Physics, Sejong University, Seoul, South Korea

²² Department of Physics, University of Oslo, Oslo, Norway

²³ Dipartimento di Elettrotecnica ed Elettronica del Politecnico, Bari, Italy

²⁴ Dipartimento di Fisica dell’Università ‘La Sapienza’ and Sezione INFN, Rome, Italy

²⁵ Dipartimento di Fisica dell’Università and Sezione INFN, Cagliari, Italy

²⁶ Dipartimento di Fisica dell’Università and Sezione INFN, Trieste, Italy

²⁷ Dipartimento di Fisica dell’Università and Sezione INFN, Turin, Italy

²⁸ Dipartimento di Fisica e Astronomia dell’Università and Sezione INFN, Bologna, Italy

²⁹ Dipartimento di Fisica e Astronomia dell’Università and Sezione INFN, Catania, Italy

³⁰ Dipartimento di Fisica e Astronomia dell’Università and Sezione INFN, Padova, Italy

³¹ Dipartimento di Fisica ‘E.R. Caianiello’ dell’Università and Gruppo Collegato INFN, Salerno, Italy

³² Dipartimento di Scienze e Innovazione Tecnologica dell’Università del Piemonte Orientale and Gruppo Collegato INFN, Alessandria, Italy

³³ Dipartimento Interateneo di Fisica ‘M. Merlin’ and Sezione INFN, Bari, Italy

³⁴ Division of Experimental High Energy Physics, University of Lund, Lund, Sweden

³⁵ Eberhard Karls Universität Tübingen, Tübingen, Germany

³⁶ European Organization for Nuclear Research (CERN), Geneva, Switzerland

³⁷ Excellence Cluster Universe, Technische Universität München, Munich, Germany

³⁸ Faculty of Engineering, Bergen University College, Bergen, Norway

³⁹ Faculty of Mathematics, Physics and Informatics, Comenius University, Bratislava, Slovakia

⁴⁰ Faculty of Nuclear Sciences and Physical Engineering, Czech Technical University in Prague, Prague, Czech Republic

⁴¹ Faculty of Science, P.J. Šafárik University, Košice, Slovakia

⁴² Faculty of Technology, Buskerud and Vestfold University College, Vestfold, Norway

⁴³ Frankfurt Institute for Advanced Studies, Johann Wolfgang Goethe-Universität Frankfurt, Frankfurt, Germany

⁴⁴ Gangneung-Wonju National University, Gangneung, South Korea

⁴⁵ Gauhati University, Department of Physics, Guwahati, India

⁴⁶ Helsinki Institute of Physics (HIP), Helsinki, Finland

⁴⁷ Hiroshima University, Hiroshima, Japan

⁴⁸ Indian Institute of Technology Bombay (IIT), Mumbai, India

⁴⁹ Indian Institute of Technology Indore, Indore (IITI), India

⁵⁰ Inha University, Incheon, South Korea

⁵¹ Institut de Physique Nucléaire d’Orsay (IPNO), Université Paris-Sud, CNRS-IN2P3, Orsay, France

⁵² Institut für Informatik, Johann Wolfgang Goethe-Universität Frankfurt, Frankfurt, Germany

⁵³ Institut für Kernphysik, Johann Wolfgang Goethe-Universität Frankfurt, Frankfurt, Germany

⁵⁴ Institut für Kernphysik, Westfälische Wilhelms-Universität Münster, Münster, Germany

⁵⁵ Institut Pluridisciplinaire Hubert Curien (IPHC), Université de Strasbourg, CNRS-IN2P3, Strasbourg, France

⁵⁶ Institute for Nuclear Research, Academy of Sciences, Moscow, Russia

⁵⁷ Institute for Subatomic Physics of Utrecht University, Utrecht, Netherlands

- 58 Institute for Theoretical and Experimental Physics, Moscow, Russia
59 Institute of Experimental Physics, Slovak Academy of Sciences, Košice, Slovakia
60 Institute of Physics, Academy of Sciences of the Czech Republic, Prague, Czech Republic
61 Institute of Physics, Bhubaneswar, India
62 Institute of Space Science (ISS), Bucharest, Romania
63 Instituto de Ciencias Nucleares, Universidad Nacional Autónoma de México, Mexico City, Mexico
64 Instituto de Física, Universidad Nacional Autónoma de México, Mexico City, Mexico
65 IThemba LABS, National Research Foundation, Somerset West, South Africa
66 Joint Institute for Nuclear Research (JINR), Dubna, Russia
67 Konkuk University, Seoul, South Korea
68 Korea Institute of Science and Technology Information, Daejeon, South Korea
69 KTO Karatay University, Konya, Turkey
70 Laboratoire de Physique Corpusculaire (LPC), Clermont Université, Université Blaise Pascal, CNRS-IN2P3, Clermont-Ferrand, France
71 Laboratoire de Physique Subatomique et de Cosmologie, Université Grenoble-Alpes, CNRS-IN2P3, Grenoble, France
72 Laboratori Nazionali di Frascati, INFN, Frascati, Italy
73 Laboratori Nazionali di Legnaro, INFN, Legnaro, Italy
74 Lawrence Berkeley National Laboratory, Berkeley, CA, United States
75 Moscow Engineering Physics Institute, Moscow, Russia
76 Nagasaki Institute of Applied Science, Nagasaki, Japan
77 National Centre for Nuclear Studies, Warsaw, Poland
78 National Institute for Physics and Nuclear Engineering, Bucharest, Romania
79 National Institute of Science Education and Research, Bhubaneswar, India
80 National Research Centre Kurchatov Institute, Moscow, Russia
81 Niels Bohr Institute, University of Copenhagen, Copenhagen, Denmark
82 Nikhef, Nationaal instituut voor subatomaire fysica, Amsterdam, Netherlands
83 Nuclear Physics Group, STFC Daresbury Laboratory, Daresbury, United Kingdom
84 Nuclear Physics Institute, Academy of Sciences of the Czech Republic, Řež u Prahy, Czech Republic
85 Oak Ridge National Laboratory, Oak Ridge, TN, United States
86 Petersburg Nuclear Physics Institute, Gatchina, Russia
87 Physics Department, Creighton University, Omaha, NE, United States
88 Physics Department, Panjab University, Chandigarh, India
89 Physics Department, University of Athens, Athens, Greece
90 Physics Department, University of Cape Town, Cape Town, South Africa
91 Physics Department, University of Jammu, Jammu, India
92 Physics Department, University of Rajasthan, Jaipur, India
93 Physik Department, Technische Universität München, Munich, Germany
94 Physikalisches Institut, Ruprecht-Karls-Universität Heidelberg, Heidelberg, Germany
95 Purdue University, West Lafayette, IN, United States
96 Pusan National University, Pusan, South Korea
97 Research Division and ExtreMe Matter Institute EMMI, GSI Helmholtzzentrum für Schwerionenforschung, Darmstadt, Germany
98 Rudjer Bošković Institute, Zagreb, Croatia
99 Russian Federal Nuclear Center (VNIIEF), Sarov, Russia
100 Saha Institute of Nuclear Physics, Kolkata, India
101 School of Physics and Astronomy, University of Birmingham, Birmingham, United Kingdom
102 Sección Física, Departamento de Ciencias, Pontificia Universidad Católica del Perú, Lima, Peru
103 Sezione INFN, Bari, Italy
104 Sezione INFN, Bologna, Italy
105 Sezione INFN, Cagliari, Italy
106 Sezione INFN, Catania, Italy
107 Sezione INFN, Padova, Italy
108 Sezione INFN, Rome, Italy
109 Sezione INFN, Trieste, Italy
110 Sezione INFN, Turin, Italy
111 SSC IHEP of NRC Kurchatov institute, Protvino, Russia
112 Stefan Meyer Institut für Subatomare Physik (SMI), Vienna, Austria
113 SUBATECH, Ecole des Mines de Nantes, Université de Nantes, CNRS-IN2P3, Nantes, France
114 Suranaree University of Technology, Nakhon Ratchasima, Thailand
115 Technical University of Košice, Košice, Slovakia
116 Technical University of Split FESB, Split, Croatia
117 The Henryk Niewodniczanski Institute of Nuclear Physics, Polish Academy of Sciences, Cracow, Poland
118 The University of Texas at Austin, Physics Department, Austin, TX, USA
119 Universidad Autónoma de Sinaloa, Culiacán, Mexico
120 Universidade de São Paulo (USP), São Paulo, Brazil
121 Universidade Estadual de Campinas (UNICAMP), Campinas, Brazil
122 University of Houston, Houston, TX, United States
123 University of Jyväskylä, Jyväskylä, Finland
124 University of Liverpool, Liverpool, United Kingdom
125 University of Tennessee, Knoxville, TN, United States
126 University of the Witwatersrand, Johannesburg, South Africa
127 University of Tokyo, Tokyo, Japan
128 University of Tsukuba, Tsukuba, Japan
129 University of Zagreb, Zagreb, Croatia
130 Université de Lyon, Université Lyon 1, CNRS/IN2P3, IPN-Lyon, Villeurbanne, France
131 V. Fock Institute for Physics, St. Petersburg State University, St. Petersburg, Russia
132 Variable Energy Cyclotron Centre, Kolkata, India
133 Warsaw University of Technology, Warsaw, Poland
134 Wayne State University, Detroit, MI, United States
135 Wigner Research Centre for Physics, Hungarian Academy of Sciences, Budapest, Hungary
136 Yale University, New Haven, CT, United States

¹³⁷ Yonsei University, Seoul, South Korea

¹³⁸ Zentrum für Technologietransfer und Telekommunikation (ZTT), Fachhochschule Worms, Worms, Germany

ⁱ Deceased.

ⁱⁱ Also at: Georgia State University, Atlanta, Georgia, United States.

ⁱⁱⁱ Also at: Department of Applied Physics, Aligarh Muslim University, Aligarh, India.

^{iv} Also at: M.V. Lomonosov Moscow State University, D.V. Skobeltsyn Institute of Nuclear Physics, Moscow, Russia.